ULTRAFAST SILICON-BASED MODULATORS USING OPTICAL SWITCHING OF VANADIUM O2

Sharon Weiss
VANDERBILT UNIVERSITY

12/04/2014
Final Report

REPORT DOCUMENTATION PAGE

1. REPORT DATE *(DD-MM-YYYY)*	2. REPORT TYPE	3. DATES COVERED *(From - To)*

4. TITLE AND SUBTITLE

5a. CONTRACT NUMBER

5b. GRANT NUMBER

5c. PROGRAM ELEMENT NUMBER

6. AUTHOR(S)

5d. PROJECT NUMBER

5e. TASK NUMBER

5f. WORK UNIT NUMBER

7. PERFORMING ORGANIZATION NAME(S) AND ADDRESS(ES)

8. PERFORMING ORGANIZATION REPORT NUMBER

9. SPONSORING / MONITORING AGENCY NAME(S) AND ADDRESS(ES)

10. SPONSOR/MONITOR'S ACRONYM(S)

11. SPONSOR/MONITOR'S REPORT NUMBER(S)

12. DISTRIBUTION / AVAILABILITY STATEMENT

13. SUPPLEMENTARY NOTES

14. ABSTRACT

15. SUBJECT TERMS

16. SECURITY CLASSIFICATION OF:			17. LIMITATION OF ABSTRACT	18. NUMBER OF PAGES	19a. NAME OF RESPONSIBLE PERSON
a. REPORT	b. ABSTRACT	c. THIS PAGE			19b. TELEPHONE NUMBER *(include area code)*

Ultrafast Silicon-based Modulators using Optical Switching of Vanadium Dioxide

Sharon M. Weiss

Department of Electrical Engineering and Computer Science, Vanderbilt University
sharon.m.weiss@vanderbilt.edu

Richard F. Haglund, Jr.

Department of Physics and Astronomy, Vanderbilt University
richard.haglund@vanderbilt.edu

In this report, we describe our accomplishments during this project in four areas: (1) optical switching of Si-VO$_2$ ring resonators and Mach-Zehnder interferometers; (2) nanosecond all-optical switching of Si-VO$_2$ absorption modulators and ring resonators; (3) nanosecond electrical switching of Si-VO2 absorption modulators; and (4) designs for fiber-to-chip couplers and alternative modulator geometries. The operation of the Si-VO$_2$ modulator is initially demonstrated by using photothermal heating to induce the VO$_2$ semiconductor-to-metal phase transition and modulate the transmitted optical signal intensity. Ultrafast, all-optical switching at the nanosecond time scale is then demonstrated by using a pulsed nanosecond laser for excitation. Ultrafast electro-optic switching is also demonstrated at the nanosecond time scale using a geometry that would allow for straightforward integration with existing optical interconnect technologies. Finally, extensions to the Si-VO$_2$ modulator are presented for increased efficiency of source-to-modulator coupling using a transformation optics design approach and increased quality factor-to-mode volume ratio using a slotted nanocavity design.

Statement of Objective and Summary of Outcomes: The overall objective of this project was to develop reconfigurable photonic devices based on the integration of vanadium dioxide (VO$_2$) with silicon waveguide structures to enable of a new generation of silicon-compatible optical circuits operating at THz speeds. By utilizing the sub-picosecond semiconductor-to-metal transition (SMT) in VO$_2$ as the active switching mechanism that enables direct modulation of the effective index of silicon waveguides, hybrid Si-VO$_2$ structures have the potential to overcome intrinsic limits in the optical response of silicon while maintaining compatibility with existing silicon microelectronic architectures. Record values of optically induced broadband in-line absorption modulation (~4 dB μm^{-1}) and intracavity phase modulation (~$\pi/5$ rad μm^{-1}) were achieved at nanosecond time scales (limited by the FWHM of the excitation laser) with optical modulation depths in excess of 7 dB from high-bandwidth (>100 GHz) hybrid structures. Record low switching times < 2ns (possibly limited by the experimental setup) for the electrically induced SMT of VO$_2$ were shown on hybrid Si-VO$_2$ absorption modulators, which represents the first demonstration of electro-optic switching using the electrically triggered SMT of VO$_2$.

1. Optical switching of Si-VO$_2$ ring resonators and Mach-Zehnder interferometers

(1) Ring resonators

The Si-VO$_2$ hybrid micro-ring resonator structure was fabricated on a silicon-on-insulator (SOI) substrate with a 220nm p-type, 14–22 Ω cm resistivity, Si(100) layer and 1 µm buried oxide layer (SOITEC). Electron-beam lithography (JEOL JBX-9300–100kV) was performed using ZEP 520A e-beam resist spun at 6,000 rpm (~300nm thick). After pattern exposure and development in xylenes for 30s followed by an IPA rinse and N$_2$ drying, anisotropic reactive-ion etching was performed (Oxford PlasmaLab 100) using C$_4$F$_8$/SF$_6$/Ar process gases to completely etch the exposed portion of the 220nm Si layer.

A second stage of electron-beam lithography (Raith eLine) was performed to open windows for VO$_2$ deposition, using ZEP 520A spun at 2,000 rpm (~500nm thick) to better facilitate VO$_2$ lift-off. Amorphous VO$_x$ was then deposited by electron-beam vaporization of VO$_2$ powder (100 mesh, 99.5% purity) in an Ångstrom Engineering deposition system. After deposition, lift-off in acetone under ultra-sonication was performed, leaving behind amorphous VO$_x$ patches across the silicon rings. Samples were then annealed in a vacuum chamber with 250 mTorr of oxygen at 450°C for five minutes to yield polycrystalline, switching VO$_2$ patches.

The fabricated device structure is shown in the scanning electron microscopy (SEM) image in Fig. 1a [1]. The radius of the ring, measured to the center of the ring waveguide, is 1.5µm. The ring waveguide width is ~500nm while the bus waveguide width is slightly reduced to ~400nm to promote better phase matching. A coupling gap of ~75nm is employed to achieve near-critical coupling. Note that a top air cladding is used in this structure and all subsequent measurements. A ~560nm long patch of nanocrystalline VO$_2$ with a low-apparent roughness covers a small portion of the ring. Profilometry measurements revealed the VO$_2$ film thickness to be ~70nm. The quality of the VO$_2$ film was evaluated by temperature-dependent reflectance measurements on witness samples that consisted of VO$_2$ films deposited on Si(100) substrates at the same time and under the same conditions as the device structures. Figure 1b reveals the hysteresis behavior in optical reflectivity, measured using a white-light source and silicon photo-detector. As the film temperature is increased beyond a critical temperature, ~63°C, a dramatic increase in reflectivity is observed, indicating initiation of the transition between semiconducting and metallic phases. The steep slope, high contrast, and relatively narrow hysteresis exhibited by these reflectivity measurements indicate the high quality of the deposited VO$_2$ films [2].
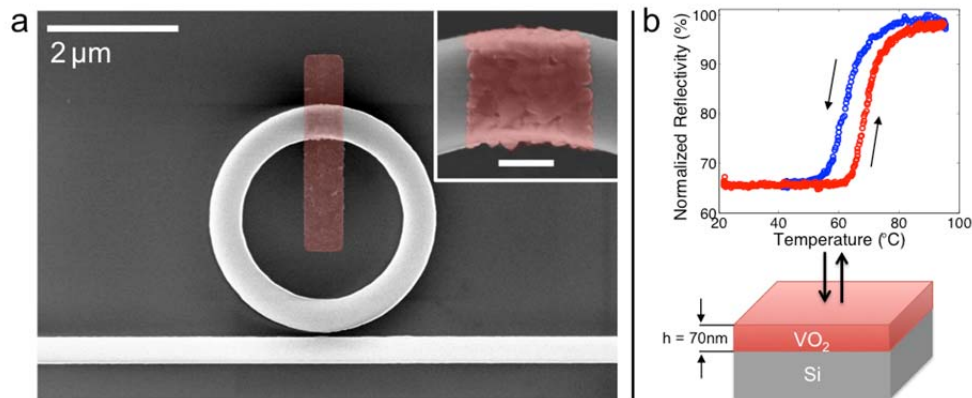

Fig. 1. (a) SEM image of a hybrid Si-VO$_2$ micro-ring resonator with 1.5µm radius. The lithographically placed VO$_2$ patch is highlighted in false-color. (Inset scale bar is 250nm). (b) White-light reflectivity versus temperature on a thin film VO$_2$ control sample deposited on a Si(100) substrate. Adapted from [1].

Passive transmission measurements of hybrid Si-VO$_2$ ring resonators were performed to characterize the structures. In preparation for the optical measurements, samples were cleaved across each end of the bus waveguide, several millimeters away from the central device, and mounted on an XY positioning stage. Piezo-controled XYZ stages were used to position and couple light to/from polarization-maintaining lensed fibers (OZ Optics Ltd.) as shown in Fig. 2a. A tunable cw laser (Santec TSL-510) was used as the probe in passive transmission measurements, utilizing quasi-TE polarization, over the wavelength range 1500–1630nm.

In Fig. 2b, the transmission of two 1.5μm radius ring-resonators with and without integration of VO$_2$ are compared. Both devices exhibit a very large free-spectral range (FSR) near 60nm, which is highly desirable for enabling multiplexed photonic architectures. Taking the average FSR values and resonance positions, we estimate group indices of ~4.385 and ~4.415 for the all-Si and hybrid Si-VO$_2$ resonators, respectively. Note that in the case of the hybrid resonator, the measured group index comprises contributions from both the bare-Si and VO$_2$-coated sections. Thus, when taking into account the ~6% VO$_2$ coverage on the ring, we approximate a group index closer to ~4.9 for the VO$_2$ coated section of the ring waveguide. Further, we find that the Si-VO$_2$ hybrid resonator has deeper resonances than the Si-only devices, which suggests near-critical coupling. This result is deliberately achieved by initially over-coupling the all-Si resonator by the use of the small ~75nm air gap. Introduction of the small VO$_2$ patch increases the round trip loss, primarily due to the modal mismatch between the bare-Si ring waveguide and hybrid VO$_2$-coated waveguide sections.
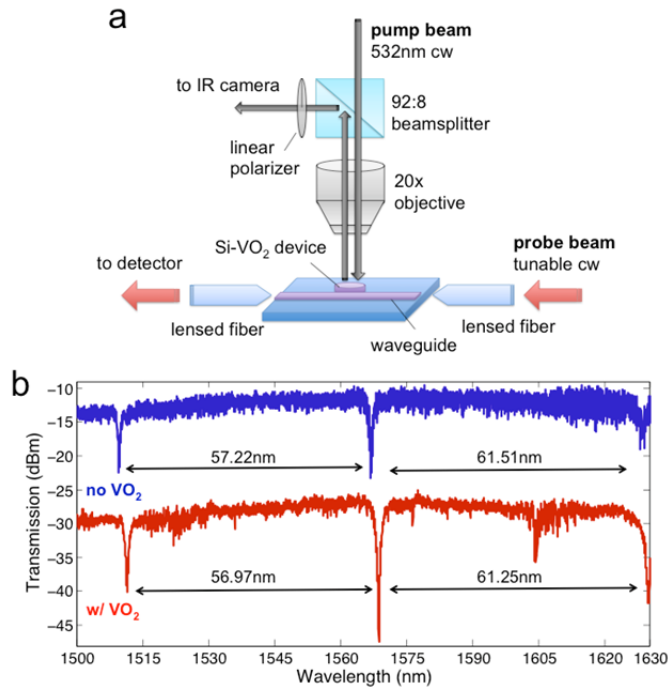
Fig. 2. (a) Schematic of the optical measurement set-up. (b) Passive spectral measurements of optical transmission on 1.5μm radius micro-ring resonators with (bottom) and without (top) an integrated VO$_2$ patch. For clarity, the top all-Si curve has been offset by +20dBm. Adapted from [1].

To characterize the active optical response of the hybrid Si-VO$_2$ micro-ring resonator, a 532nm cw pump laser (New Focus 3951-20) was focused onto the device with a 20x objective as shown in Fig. 2a. An infrared (IR) camera was used for alignment purposes. IR imaging at

maximum exposure and contrast settings was used to determine an upper bound for the Gaussian beam size, $w_0 \approx 90\mu m$. Given that nearly 100% of the total power (P_{total}) is contained within the radius $2w_0$, we estimate the average intensity to be approximately 15 W/cm^2. The peak on-axis intensity is therefore ~30 W/cm^2. In our experiments we found that precise positioning of the pump beam, to within approximately $10\mu m$, was required to trigger the SMT, suggesting that the peak on-axis intensity may be a more reasonable indicator of the laser intensity near the Si-VO$_2$ micro-ring.

In Fig. 3, we present the optical transmission of the $1.5\mu m$ radius hybrid Si-VO$_2$ ring resonator as measured before and after triggering the SMT with the 532nm pump laser. These measurements reveal a sizeable shift $\Delta\lambda = -1.26$nm in the resonance wavelength, coinciding with an optical modulation greater than 10dB at the initial resonance position, $\lambda = 1568.78$nm. Because VO$_2$ exhibits a dramatically reduced refractive index in the metallic state, a blue-shift in resonance frequency is naturally expected to arise from triggering the SMT. However, additional effects are also expected to be present during this experiment, including dependence on: (1) the thermo-optic (TO) effect in silicon, $\Delta n/\Delta T = +1.86\times10^{-4}$/K [3], and (2) the free-carrier index (FCI) [4]. These two effects are substantially weaker than the much larger optical response of the VO$_2$ and, in this experiment, also carry opposite signs. Thus, the photothermal approach for triggering VO$_2$'s SMT enables silicon's TO and FCI refractive index contributions to be used against each other so that the optical signature of VO$_2$ can be more readily distinguished. We verified that the dominant contribution to this resonance shift was indeed coming from the VO$_2$ by performing a control experiment on an all-Si micro-ring with the same dimensions, revealing a $\Delta\lambda = +0.938$nm net red-shift in resonance wavelength. This indicates that in the absence of TO or FCI effects, the achievable resonance blue-shift arising solely from VO$_2$'s SMT is even larger than the net $\Delta\lambda = -1.26$nm value reported from this experiment.
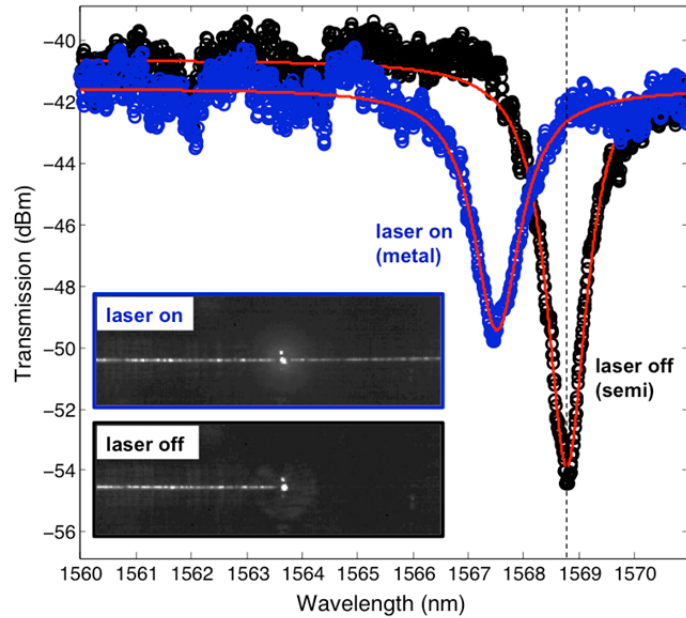

Fig. 3. Optical transmission of the $1.5\mu m$ radius hybrid Si-VO$_2$ ring resonator as a function of wavelength, before and after triggering the SMT with a 532nm pump laser. The lines are Lorentzian fits. Inset: IR camera images revealing vertical radiation at a fixed probe wavelength, $\lambda = 1568.78$nm (dashed line). Adapted from [1].

Figure 4 illustrates the time-dependent optical response at the fixed probe wavelength $\lambda = 1568.78$nm. When VO_2 is in the semiconducting state, this wavelength corresponds to being 'on-resonance', and thus the initial optical transmission is very low. Illuminating the device with the 532nm pump laser results in an immediate increase in the optical transmission followed by a ~15s decay toward low transmission and then an increase toward high transmission lasting about 3 min (Fig. 4a). This time-dependent optical response can be explained entirely in the context of laser-induced heating. The initial spike to high transmission results from rapid heating of the silicon ring and a thermo-optic dominated shift to longer resonance wavelength. However, once the SMT threshold temperature is approached, the resonance immediately begins to blue-shift back toward its original position and beyond, effectively sweeping across the resonance and producing a dip and rise in transmission. The photothermal approach for triggering the SMT taken in this experiment (Fig. 2a) can be tuned to reduce response time by over three orders of magnitude by increasing the pump intensity [5]. As we describe in the next section of this report, increasing the pump intensity through nanosecond pulsed lasers allows for faster optical switching times that are limited by the pump pulse width rather than the intrinsic sub-ps time scale of the VO_2 SMT.

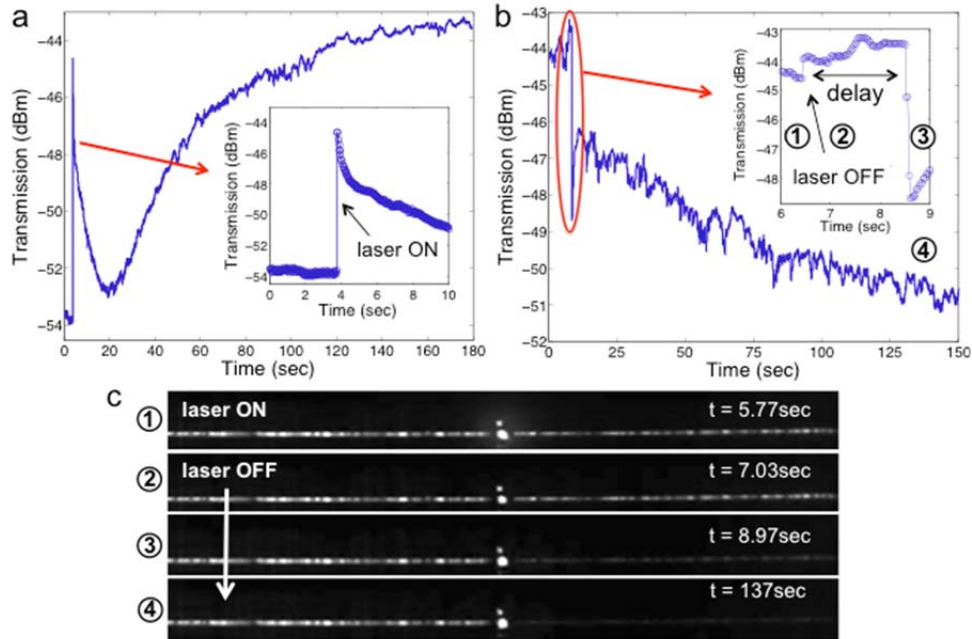Fig. 4. Optical transmission as a function of time at $\lambda = 1568.78$nm, in the 1.5μm radius hybrid Si-VO_2 device, when turning the 532nm pump laser (a) ON and (b) OFF. (c) Infrared camera images highlighting the delayed probe response observed in (b). Adapted from [1].

In Fig. 4b,c we examine the optical response, again at $\lambda = 1568.78$nm, after turning off (*i.e.* blocking) the 532nm pump laser. When this occurs, the device immediately begins cooling off, ultimately resulting in a return to the VO_2 semiconducting state and an 'on-resonance' level of low transmission. However, an immediate drop in transmission is not observed; rather, turning off the laser coincides with a very small (~0.5dB) increase in transmission followed by a ~2s delay before a dramatic, ~2-5dB, drop in transmission. The initial increase, which was repeatedly observed during multiple experiments, might possibly be attributed to either a small TO shift from the cooling silicon ring waveguide or to the recombination of photo-generated

carriers in the silicon, which would eliminate free-carrier absorption effects. Most importantly however, we attribute the ~2s delay to device cooling at temperatures above the threshold SMT temperature. Once the threshold temperature is reached, the transition between metallic and semiconducting states is triggered. The ~2s delay between the pump shut-off and large probe response is similarly observed using the IR camera (Fig. 4c), and is strong evidence that a complete SMT indeed takes place prior to blocking the pump laser beam. After crossing the metal-to-semiconductor threshold temperature, the device requires several more minutes to cool completely back to room temperature. We note that this cooling time-scale was not fundamental to the phase transition, but was rather a function of our experimental configuration and the absence of well-designed heat dissipation components in this proof-of-concept experiment.

The slow, photothermal switching of the Si-VO$_2$ ring resonators discussed in this section laid an important foundation for our project. We established a fabrication procedure that led to high quality resonances for the hybrid ring resonators and we demonstrated that the SMT of VO$_2$ could be used to dynamically modulate the intensity of the transmitted optical signal.

(2) Mach-Zehnder Interferometers (MZIs)

MZI devices were fabricated using an unbalanced geometry adapted from Ref. [6], as shown in Fig. 5a. The unbalanced structure features a 'built in' optical path length difference, producing interference fringes and sharp spectral features which are favorable for performing sensitive measurements of phase or refractive index with an improved signal-to-noise ratio. Figure 5b shows the experimental results for photothermally switching a hybrid MZI with a $L_0 = 100$ μm path length offset and a VO$_2$ patch length $L_{VO2} = 2$ μm [7]. Photothermal switching was performed with a continuous wave laser, similar to the ring resonator experiments described above. The transmission spectra show a clear blueshift of the interference fringes, as well as reduced fringe amplitude. Analysis of the transmission spectrum revealed a phase shift of $\Delta\Phi \approx -0.584$ rad, an effective index change of $\Delta n \approx -0.07$, and an intensity modulation of ≈ 0.156 due to the VO$_2$ SMT occurring in the active arm of the MZI. Considering the 2 μm VO$_2$ patch length employed in this study, the change in transmission corresponds to a large absorption modulation value of 4 dB/μm. Although very large extinction ratios can be achieved with the Si-VO$_2$ MZI geometry, the necessarily long VO$_2$ patch lengths that would be required would result in large insertion losses for the structure when VO$_2$ is in the metallic state. However, we believe the MZI design is well-suited for future studies investigating the time-dependent dielectric function of VO$_2$, which has not been previously characterized.
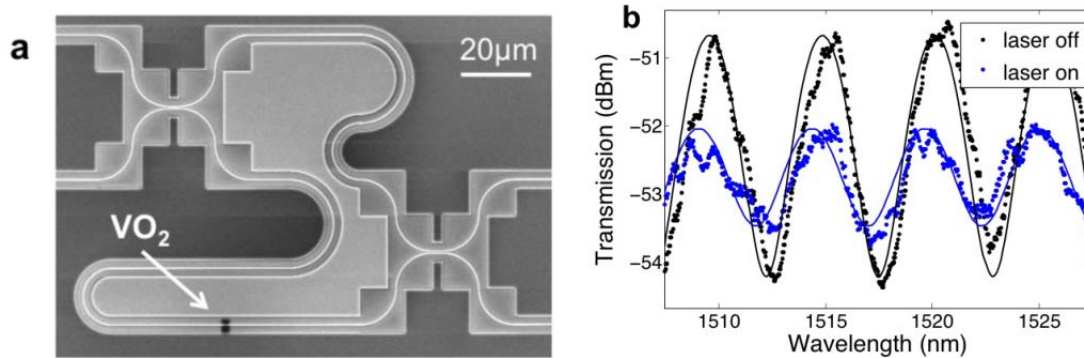

Fig. 5. (a) SEM image of unbalanced Si-VO$_2$ hybrid MZI. (b) Transmission spectra of MZI with VO$_2$ in the semiconducting (laser off) and metallic (laser on) states. Adapted from [7].

2. Nanosecond all-optical switching of Si-VO$_2$ absorption modulators and ring resonators

After completing proof-of-concept experiments described in section 1, we strived to reduce the switching times by using a nanosecond pulsed laser to excite the VO$_2$ phase transition. As illustrated in Fig. 6, Si-VO$_2$ hybrid absorption modulators and ring resonators were fabricated to investigate their capabilities for nanosecond all-optical signal modulation [8]. We employed a nanosecond Nd:YAG pulsed laser to drive the VO$_2$ phase transition that modulated the transmission intensity of the hybrid photonic structures. The SMT of VO$_2$ dramatically alters the optical properties of the material and, as was previously mentioned, has been shown to occur on sub-picosecond timescales, comparable to the pump pulse duration down to ~75 fs [9]. For the absorption modulator configuration where a VO$_2$ patch is deposited onto a single-mode silicon waveguide, the SMT is harnessed to introduce a significant change in absorption, $\Delta\alpha$. This non-resonant configuration utilizes the large contrast in the imaginary part of the VO$_2$ refractive index, on the order of +2.6i at 1550 nm [10]. The absorption induced in the waveguide is engineered by controlling the overlap of the evanescent field with the VO$_2$ patch (i.e., waveguide dimensions and patch thickness) and by tuning the VO$_2$ patch length. For the ring resonator configuration, the large contrast in the real part of the VO$_2$ refractive index, approximately -1.06 at 1550 nm, is used to introduce a significant change in effective index or phase $\Delta\phi$ of light in the ring. The large change in refractive index enables large changes in transmission through the ring resonator, even with ultra-compact rings (e.g., radius of 1.5 μm in our work). Both Si-VO$_2$ hybrid photonic devices were measured using the pump-probe configuration illustrated in Fig. 6c with a tunable continuous wave probe laser and a pulsed pump laser (~25 ns FWHM, 1064 nm).
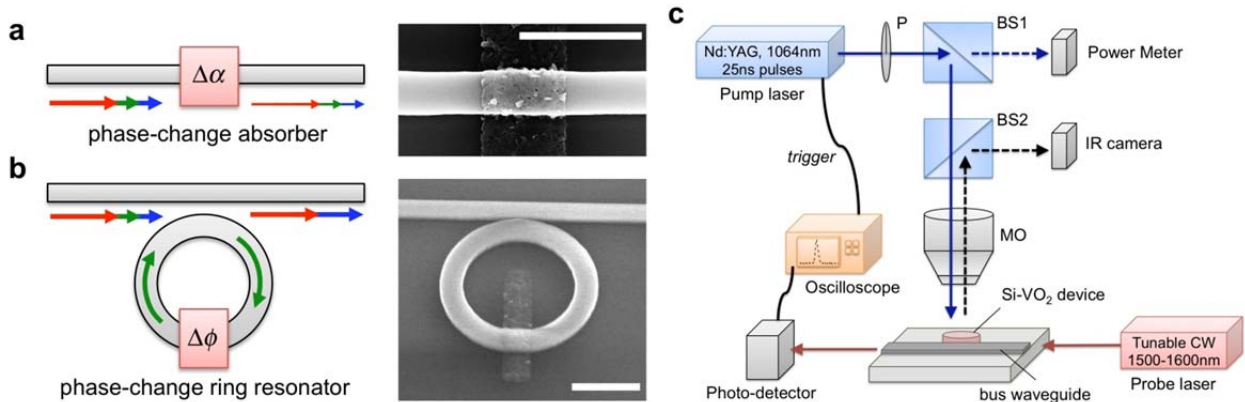

Fig. 6. (a) Illustration of a phase-change absorber where the SMT induces a broadband change in absorption $\Delta\alpha$. SEM image of a typical ultra-compact Si-VO$_2$ absorber with a 1 μm VO$_2$ patch length. (b) Illustration of a phase-change ring resonator where the SMT induces an intracavity phase modulation $\Delta\phi$. SEM image of an ultra-compact Si-VO$_2$ micro-ring resonator with radius $R = 1.5$ μm and a ~500 nm VO$_2$ patch length. Scale bars in both SEM images correspond to 1.5 μm, approximately the probe wavelength in free space. (c) Schematic of the experimental pump-probe configuration for nanosecond all-optical switching studies. Tunable probe-laser transmission is monitored with a photo-detector and oscilloscope, while nanosecond-pulsed pump light is delivered to the device through a microscope objective (MO) and two beam-splitters (B1 and B2) with power controlled by a linear polarizer (P). Adapted from [8].

Figure 7a shows the time-dependent optical transmission of the Si-VO$_2$ absorption modulators for varying pump fluences (~0.5-8 mJ cm^{-2}) and patch lengths ($L_{VO2} \sim$ 1 μm and 500 nm). An abrupt reduction in optical transmission in response to optical pumping is observed on a time-scale comparable to the pump-pulse FWHM (~25 ns), consistent with reports using ~10^{-8}-10^{-14} s laser pulses to optically trigger the SMT in VO$_2$ thin films [9, 11]. The modulation

depth increases approximately linearly with pump intensity and saturates near a threshold fluence of ~1.27 mJ/cm^2. At threshold, the modulation depth of the Si-VO$_2$ in-line absorbers is estimated to be 4 ± 0.3 dB μm^{-1}, which is approximately 40 times larger than monolayer graphene-on-Si absorbers (~0.1 dB μm^{-1}) [12] and more than three orders of magnitude larger than silicon-based two-photon cross-absorption modulation (~0.001 dB μm^{-1}) [13]. Broadband device operation was verified over a wide range of probe wavelengths, 1500-1600nm, as shown in Fig. 7c.

Figure 8a shows the transmission spectra for an ultra-compact Si-VO$_2$ hybrid micro-ring resonator, $R = 1.5$ μm, with an integrated ~500 nm long and ~70 nm thick VO$_2$ patch coating a portion of the ring waveguide. Owing primarily to bending losses at this ultra-compact ring radius, this device shows a modest Q ~ 10^3, resulting in an optical bandwidth exceeding 100 GHz. The time-dependent optical transmission for the pump-probe experiment is shown in Fig. 8b, where probe wavelength is tuned to match the resonance minimum ($\lambda = 1588.5$ nm). Photoinducing the SMT results in an abrupt increase in transmission, estimated in this case to be ~7.2 dB, followed by a slower relaxation to the low initial value. The observed modulation depth is several times larger than what can be achieved for the in-line absorber with the same active VO$_2$ area. The large increase in transmission observed for this modest Q-factor device suggests that the resonance wavelength is significantly modified by the photoinduced SMT. This is in stark contrast to conventional Si-only devices, where relatively weak electro-optic or nonlinear effects necessitate the use of high Q-factor, very narrow band (less than 5 GHz) resonators to observe significant modulation [14]. Time dependent measurements at varying probe wavelengths were also conducted to examine the spectral characteristics of the ring resonator response. With optical pumping above threshold at 1.9 mJ/cm^2, a rapid shift in resonant wavelength of approximately $\Delta\lambda = -3.07$ nm, corresponding to a resonant frequency reconfiguration of ~360 GHz, results. The associated intracavity phase modulation is estimated at ~$\pi/5$ rad μm^{-1}, while that of a Si-only device would be three orders of magnitude lower, ~$\pi/5000$ rad μm^{-1}.
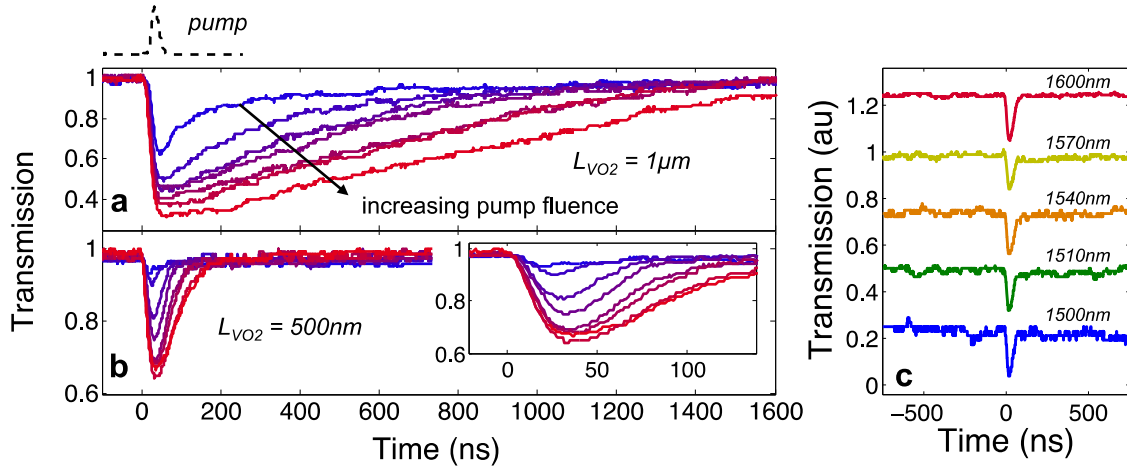
Fig. 7. Normalized probe transmission through Si-VO$_2$ absorbers with (a) 1 μm and (b) ~500 nm VO$_2$ patch lengths. The pump fluence is incrementally increased over the range ~0.5-8 mJ cm^{-2}. Inset shows a magnified view of the time response. The pump pulse is illustrated above and plotted on the same time scale. (c) Transmission through a 500 nm Si-VO$_2$ absorber for probe wavelengths ranging from 1500-1600 nm, demonstrating that the SMT of VO$_2$ can be used to realize broadband absorption modulation. Pump fluence was above threshold, ~5 mJ cm^{-2}. Plots are vertically stacked (0.25 offset) for clarity. Adapted from [8].

Fig. 8. (a) Typical resonance in the transmission spectra for a Si-VO$_2$ micro-ring resonator with radius R = 1.5μm. (b) Corresponding probe transmission where the probe wavelength is tuned to on-resonance (λ = 1588.5nm). Adapted from [8].
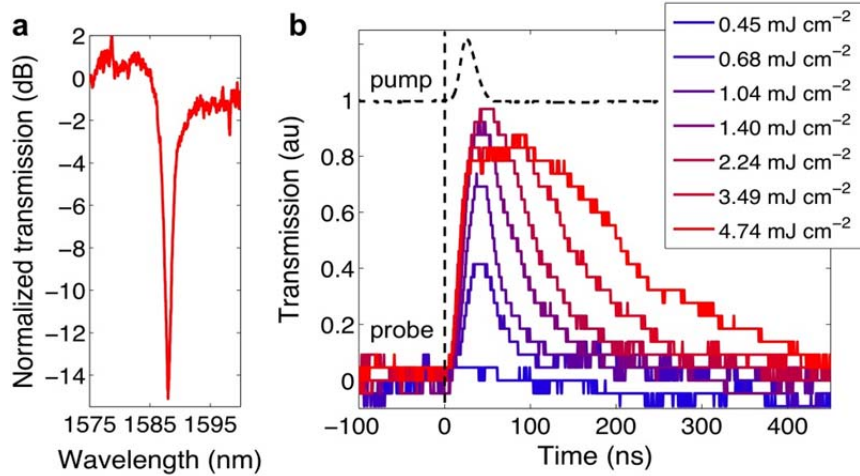
Importantly, the all-optical switching results of the Si-VO$_2$ hybrid photonic structures demonstrate record values of optically induced broadband in-line absorption modulation and intracavity phase modulation at time scales controlled by the FWHM of the pump pulse. Although the presented data shows longer relaxation times on the order of several 10s of ns, these relaxation times are not intrinsic to the phase-transition of VO$_2$ and can be controlled by a variety of factors including the thermal design, film dimensions, and method of triggering the SMT. Indeed based on the reported response times of VO$_2$ thin films optically excited with shorter pulses [11, 15, 16], it should be possible to extend device operation to ultrafast all-optical switching (less than a few ps). Recent studies touting a monoclinic metallic phase of VO$_2$ can be leveraged to ensure that only the electronic and not structural phase transition of VO$_2$ is initiated, which will significantly reduce the relaxation times of the hybrid Si-VO$_2$ modulators [17, 18].

3. Nanosecond electrical switching of Si-VO$_2$ absorption modulators

For the most direct integration into existing microelectronic architectures, Si-VO$_2$ hybrid modulators based on electrical switching may provide the lowest entry barrier. It has been previously shown that the electrical SMT can occur on nanosecond time scales in VO$_2$ films [19, 20], and on tens of picosecond time scales in V$_2$O$_3$ [21]. Based on the very recent work using V$_2$O$_3$ films that suggested thermal processes can induce the phase transition at picosecond time scales, and similar trends observed using optical terahertz-field excitation of VO$_2$ [22], there is strong reason to believe that VO$_2$ films can be electrically switched at sub-ns time scales. Here we report on our progress towards electro-optic Si-VO$_2$ hybrid modulators and the investigation of the thermal processes taking place after the initial onset of the VO$_2$ phase transition. We use the in-plane absorption modulation configuration shown in Fig. 9 with an electrical contact separation of 100 nm to ensure that a high electric field intensity is supported in the underlying 2.5 μm long VO$_2$ patch with relatively low applied voltages [23]. Sufficient field strength and electric current will induce the SMT of VO$_2$, which will drastically increase the absorption loss and reduce the transmitted intensity of light. It should be noted, however, that the trade-offs between electric field and Joule heating in the switching dynamics remain open questions, and almost certainly depend on VO$_2$ film dimensions and electrical contact geometry.
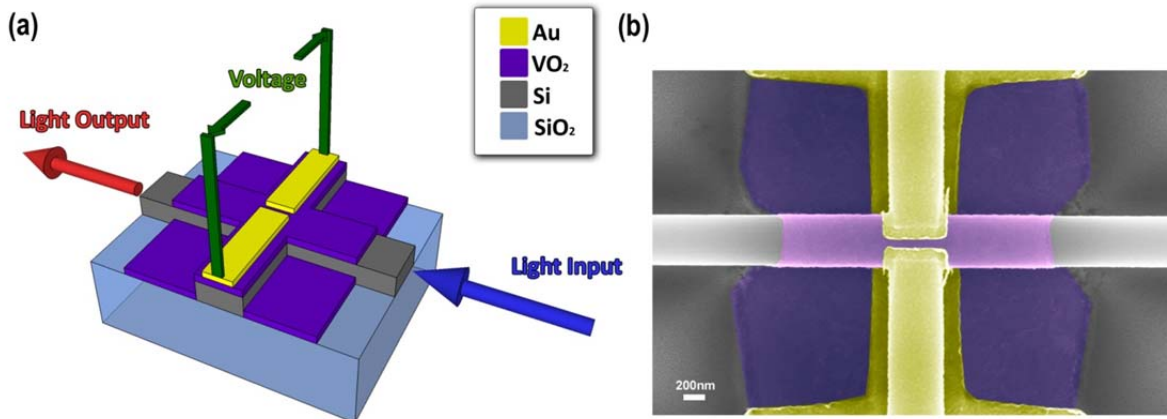
Fig. 9. (a) Device schematic representation, (b) False color SEM image of the device (VO_2 is shown in purple and gold contacts are shown in yellow).

We first characterized the electrical properties of our devices by varying the voltage and measuring the current through the device [23]. At a certain threshold voltage, a metallic current path is formed through the VO_2 and a significant jump in current is observed, as shown in Fig. 10a. COMSOL heat transfer simulations were performed to estimate the temperature increase as a result of the induced current (Fig. 10b). According to our simple model that assumes VO_2 to be in the semiconducting state, the temperature increase is negligible compared to the temperature at which the VO_2 phase transition occurs (340 K). However, our model does not take into account the increased number of carriers present injected by the applied field [21].

In order to further electrically characterize the performance of our hybrid Si-VO_2 absorption modulator, we used a function generator to supply square voltage pulses, with varying pulse amplitudes and pulse durations down to 10ns, to a simple circuit consisting of our device in series with a current limiting resistor of 50Ω (see Fig. 10c inset) [23]. The voltage across this resistor was measured and the device resistance was calculated based on the amplitude of the input voltage pulse. Figure 10c shows the time-dependent voltage measured across the current limiting resistor when two different 10ns voltage pulses are applied: one below the threshold voltage needed to induce the VO_2 phase transition and the other above threshold. The device resistance is decreased one order of magnitude (from 5kΩ to 500Ω) when the voltage is above threshold, indicating that a current path was formed through the VO_2 patch. Figure 10c also suggests that the phase transition occurs faster than our measurement setup resolution, which is less than 2ns. This electrical switching time is the fastest reported for VO_2 films. As mentioned previously, faster electrical switching times have been reported for V_2O_3 films (300ps), and there is reason to believe that the ultimate switching frequency for VO_2 is faster than 1 GHz [21].

Next, two electro-optic measurement approaches were explored to assess the modulation depth of the hybrid Si-VO_2 absorption modulator [23]. The first method involved applying square voltage pulses of varying duration and magnitude to the electrical contacts while measuring the optical transmission from the waveguide ("pulse"). A typical result is presented in Fig. 10d, where the value of the current limiting resistance is 5.1kΩ and the applied voltage is 5V for three 1s pulses followed by one 5 second pulse. A clear demonstration of electro-optic switching, a first for a VO_2–based device, is evident, albeit at very slow speed. The second method consisted of ramping up the voltage from 0V to 7V in 1V increments and then ramping the voltage back down to 0V ("steps", Fig. 11a). As expected, the relative change in transmission intensity of the hyrid Si-VO_2 absorption modulator depends on the magnitude of the applied

voltage, which relates to the switching state of the VO_2 patch between the semiconductor and metallic states. The modulation depth, defined as the ratio of the optical power in the "ON" state (0V) to the "OFF" state (voltage applied), is plotted as a function of applied voltage in Fig. 11b for both the "pulse" and "steps" methods. Good agreement is shown, and large modulation depths are achievable for sufficiently high applied voltages. The modulation depth is also a function of VO_2 patch length so higher modulation depths can be obtained at lower voltages using longer VO_2 patches. In order to control the effective length of the VO_2 patch that is switched to the metallic state, the magnitude of the current limiting series resistor was varied. As shown in Fig. 11c, at higher values of resistance, the modulation depth is very low, indicating that only a very small portion of the VO_2 patched is switched. The highest modulation depth occurs when the full patch is switched to the metallic state. The magnitude of the induced current in the device is a strong indicator of the switched fraction of the VO_2 patch. As shown in Fig. 11d, the modulation depth is directly proportional to the current, suggesting that higher current corresponds to a larger fraction of metallic state VO_2 and a larger device resistivity change. The current can be varied by changing either the series resistor or the applied voltage. Importantly, the dependence of modulation depth on current is indicative of a purely thermal process.
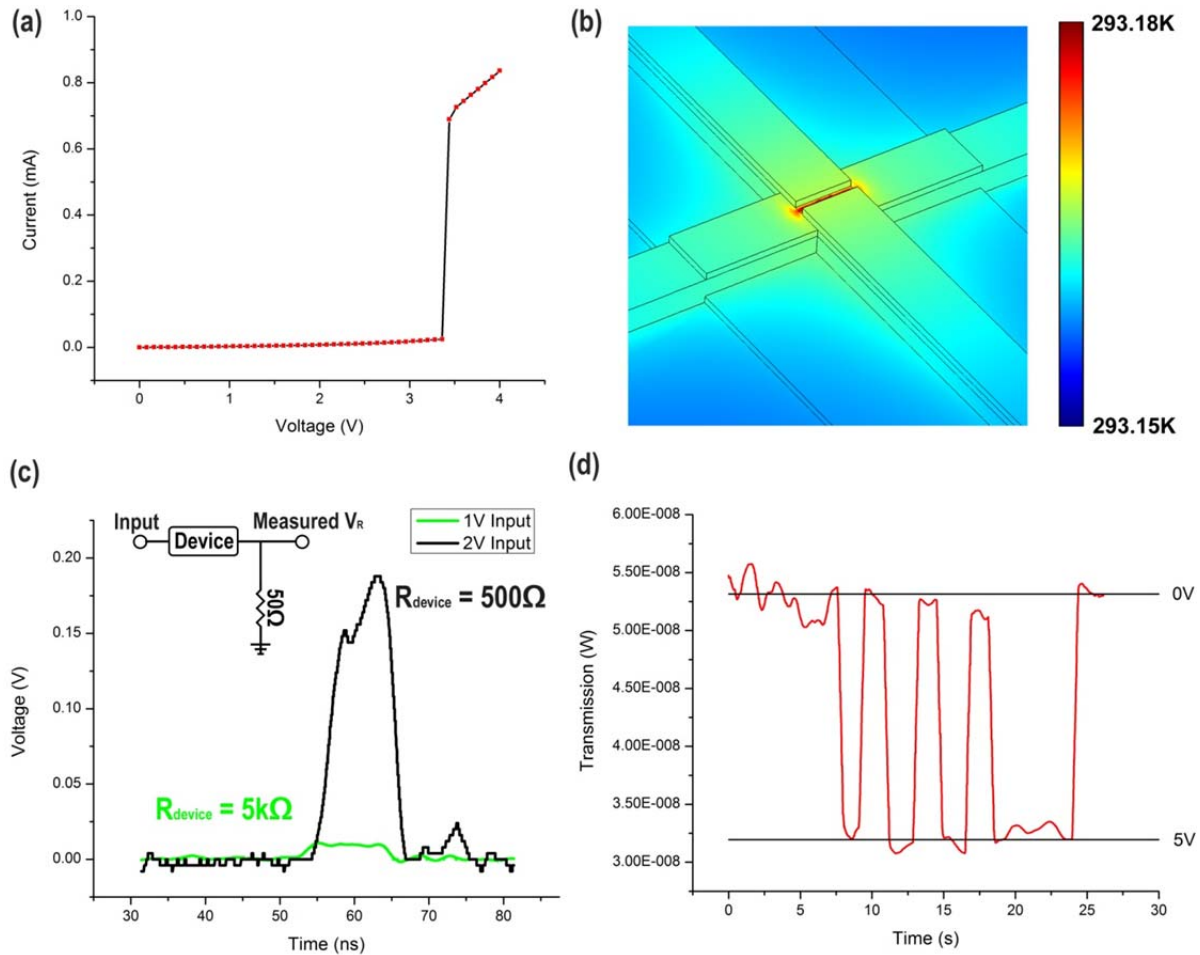
Fig. 10. (a) IV behavior of the hybrid Si-VO_2 absorption modulator, indicative of a semiconductor-to-metal transition. (b) COMSOL heat transfer simulation of the device measured in (a), assuming VO_2 is in a semiconducting state, showing negligible temperature increase caused by Joule current. (c) 10ns voltage pulse response below (green) and above (black) the switching threshold voltage. (d) Measured optical transmission as 5V pulses of various duration are applied to the electrical contacts of the device. Adapted from [23].

Fig. 11. (a) Electro-optic modulation of Si-VO$_2$ absorption modulator with staircase voltage excitation ("Steps"). (b) Dependence of modulation depth on (b) applied voltage, (c) in-series resistance, and (d) current through the device. The modulation depth is dependent on the fraction of the VO$_2$ patch that is switched to the metallic state.

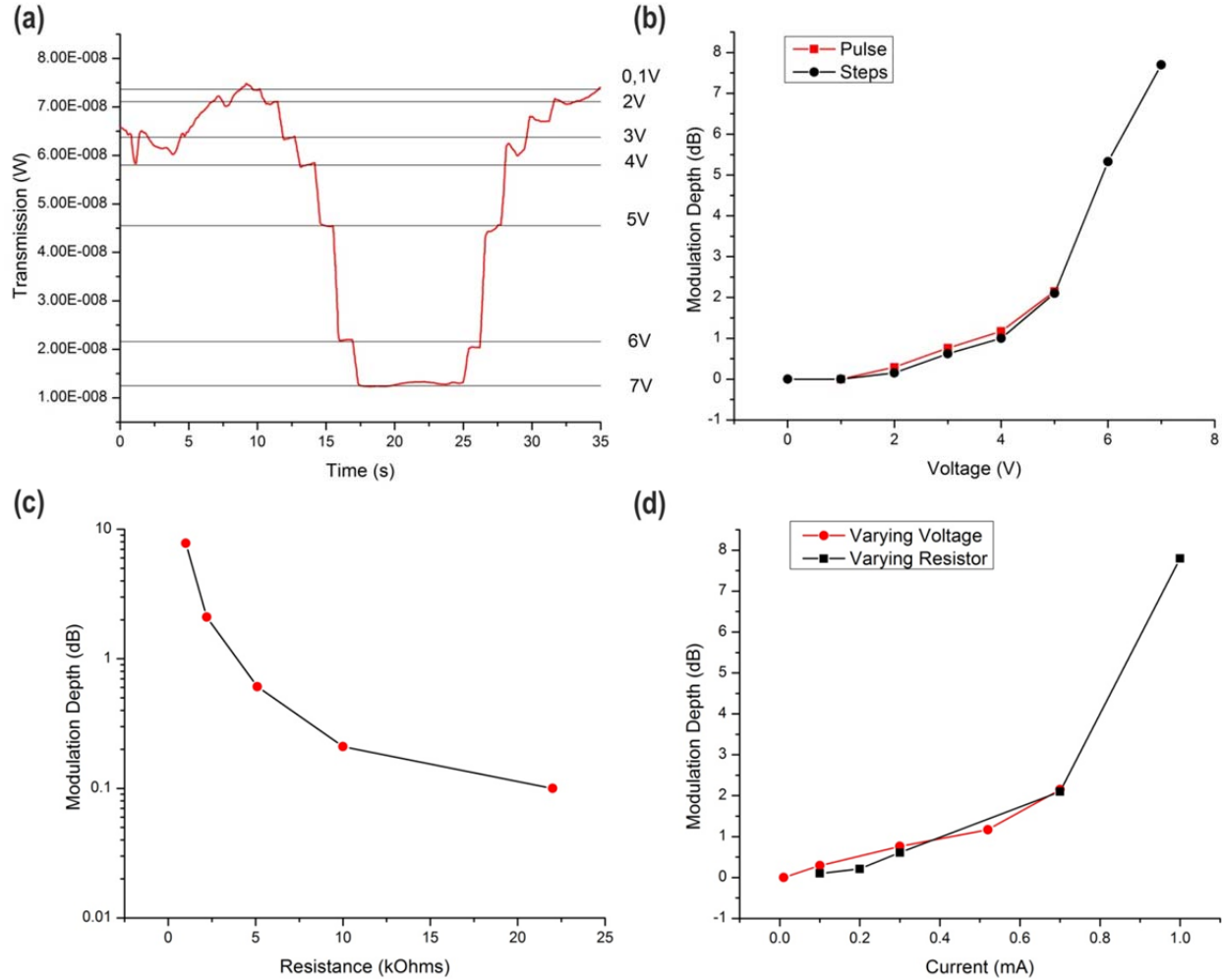Understanding the mechanism and dynamics of the electronic SMT is critical to improving device performance. The electronic SMT can be separated into two stages: the first stage is before a metallic current path is formed and the second stage is after filament formation. The first stage has been studied in the context of V$_2$O$_3$ [21] with a conclusion that a very fast thermal process (<40ps) is responsible for the initial current path formation. However, with only electrical measurements, no information can be obtained about the reverse process of the metal-to-semiconductor transition during the second stage. Our electrical measurements presented above are consistent with the V$_2$O$_3$ studies, and, importantly, our electro-optic measurements discussed below provide the opportunity to gain insight into the metal to semiconductor transition. According to our electrical measurements, a high conductivity current path forms almost immediately after an above threshold voltage is applied and the current through the device is dramatically increased, inducing rapid heating. COMSOL simulations show that a current of 1mA increases the temperature of the device to 380K, switching the entire 2.5μm long VO$_2$ patch and inducing a modulation of 7dB (as determined by 3D FDTD simulations using Lumerical$^\circledR$), which is consistent with our experimental measurements (Fig. 11d). If the current is limited by the external resistance, the modulation depth is proportional to the current and drops

to extremely low values of approximately 0.1dB (Fig. 11d). Using optical FDTD simulations, for 0.1dB modulation, we estimate the volume of the VO_2 switched to the metallic state to be approximately 100nm × 60nm × 60nm, which corresponds to a single crystal grain of VO_2 switched to a metallic state. Hence, the steady-state optical behavior of our device can be described entirely in terms of a simple thermodynamic model assuming a metallic path is already formed between the gold contacts and occurs within a single crystalline grain of VO_2.

In order to investigate the thermal processes that take place after the current path is formed, we perform optical measurements while nanosecond square voltage pulses are applied [23]. Since the electrical signal that triggers the VO_2 phase transition is completely separated from the optical probing signal, it is possible to monitor the optical transmission dynamics after the voltage is turned off, which provides critical information about the metal to semiconductor transition dynamics of VO_2. Note that for purely electrical measurements, the internal capacitance of the oscilloscope prohibits the investigation of such relaxation dynamics. In all the nanosecond optical measurements, the value of the current limiting resistor was chosen to be 2.7kΩ. First, the input voltage pulse duration was varied from 100ns to 900ns with the pulse voltage set at 4V. Results are shown in Fig. 12a. For all the pulse durations shown, the modulation depth of ~5dB is achieved within <100ns and the recovery time is ~600ns. By matching the modulation depth to FDTD simulations, we conclude that nearly the entire 2.5µm patch of VO_2 must be switched to the metallic state. Moreover, the experimental recovery time is in good agreement with dynamic heating simulations performed using COMSOL (Fig. 12e,f).

It should be noted that the transmission starts to decrease as soon as the voltage is turned on, confirming that the high-conductivity current path formed between the electrodes is indeed metallic VO_2. In order to reduce the heating of the VO_2 patch, the voltage was reduced to 3V for a 100ns voltage pulse, which reduces the excess energy delivered to the device after VO_2 is switched to the metallic state. As shown in Figure 12b, the time-dependent optical transmission is significantly different for only a 1V change in applied voltage: the 4V pulse measurement shows purely thermal recovery while the 3V pulse measurement shows a distinct jump when the voltage is turned off, followed by a thermal recovery. A similar observation in recovery dynamics can be made by investigating shorter time duration pulses with a fixed amplitude of 4V, as shown in Fig. 12c. For these shorter applied voltage pulses, there is not enough time for the entire patch of VO_2 to heat up so the slow thermal recovery time is eliminated (20ns curve in Fig. 12c). This effect can also be observed in the 10ns pulse optical measurements shown in Fig. 12d. The modulation depth is the case of the 10ns pulse is ~0.7dB, suggesting that a 200nm × 200nm × 60nm portion of the VO_2 patch between the contacts is switched to the metallic state. This volume of VO_2 is larger than that estimated to be switched in the case of minimal current (0.1dB for 100nm × 60nm × 60nm region of VO_2), suggesting that heating still plays a role for 10ns applied voltage pulses. While it should be possible to further reduce or possibly eliminate the heating contribution by placing a larger resistor in series with the device, it would not be possible to measure the resulting optical signal due to the signal-to-noise ratio of our current measurement setup. Further investigation is required to determine the intrinsic VO_2 metal-to-semiconductor transition times, which have been widely debated and previously ranging anywhere from picoseconds to hundreds of nanoseconds depending on the switching method [8, 18-21, 24-27]; however, the Si-VO_2 electro-optic modulator is an excellent platform on which to continue these studies.
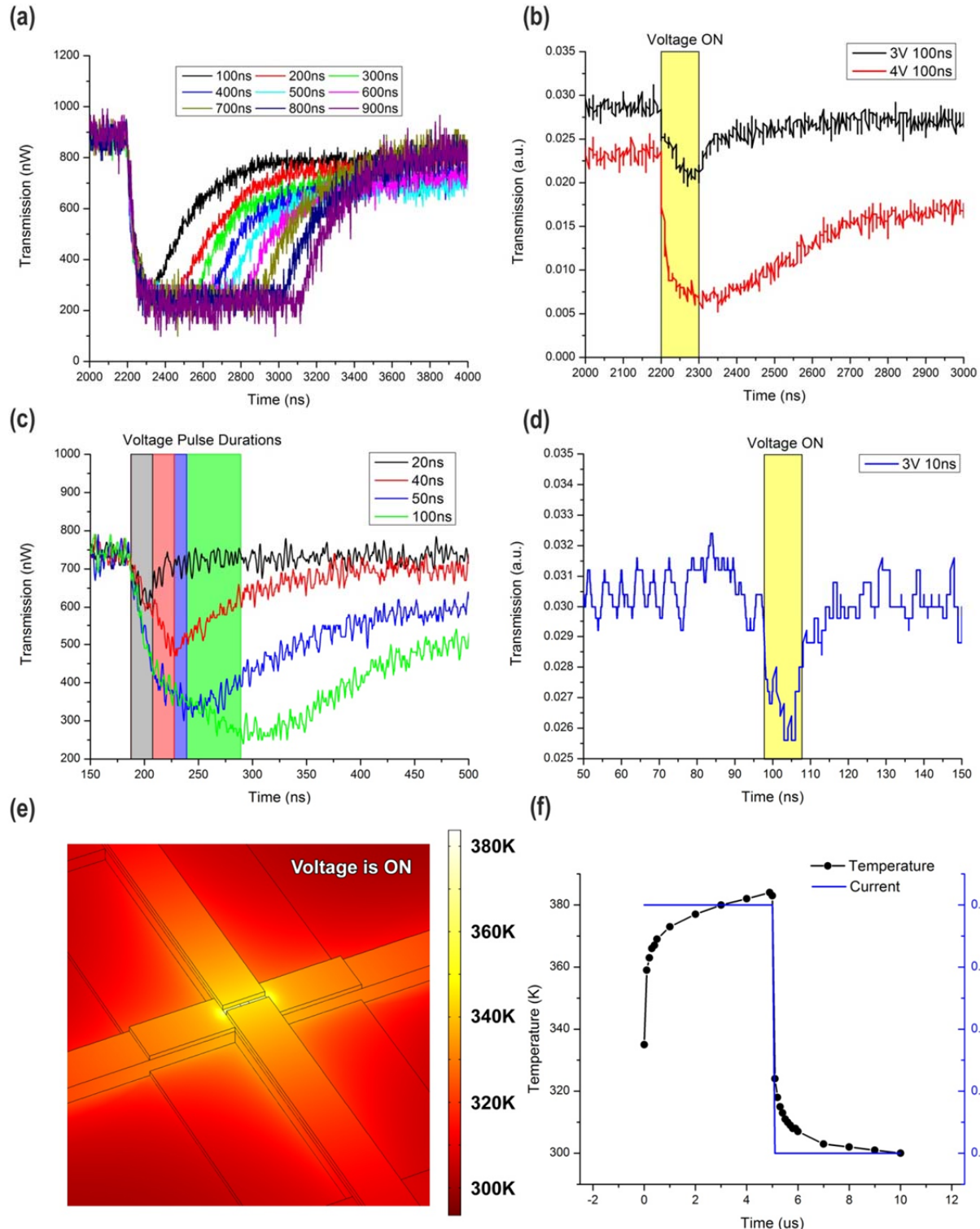
Fig. 12. (a) Optical transmission measurement of Si-VO$_2$ absorption modulator as a 4V voltage pulse of varying length (100ns-900ns) is applied to the contacts. (b) Optical transmission as a 100ns voltage pulse of varying voltage is applied. (c) Optical transmission measurement as a 4V voltage pulse of varying length (20ns-100ns) is applied. (d) Optical transmission measurement as a 3V 10ns voltage pulse is applied. (e) COMSOL heat transfer simulation 5μs after the voltage is turned on (steady-state). (f) Dynamic heating simulation using COMSOL, showing a thermal decay constant near 600 ns. Adapted from [23].

4. Designs for fiber-to-chip couplers and alternative modulator geometries
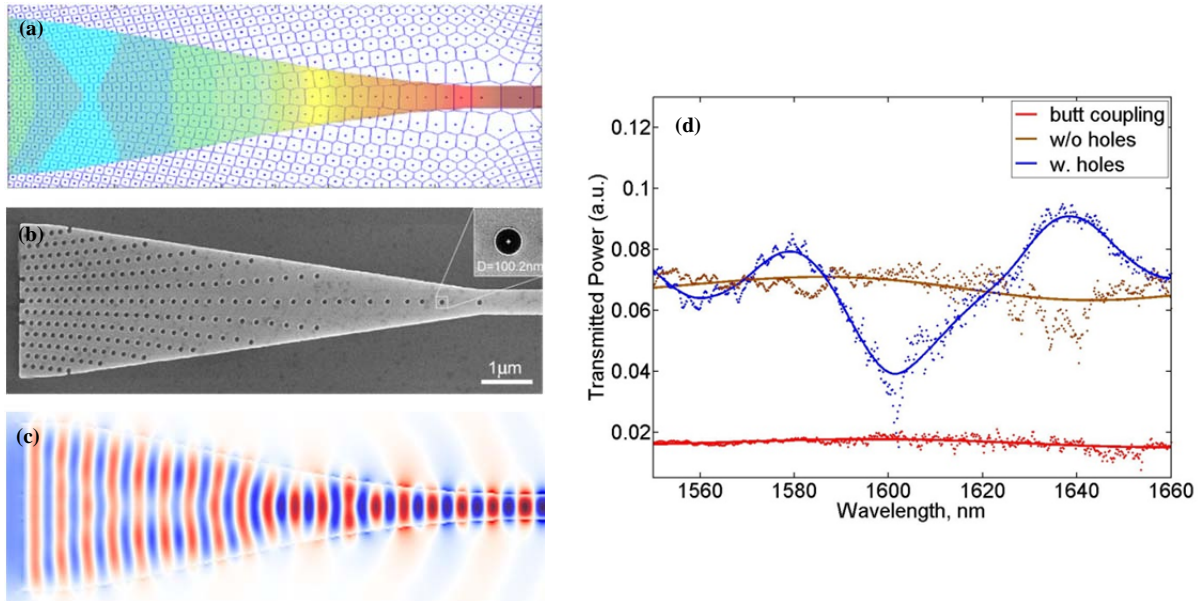
Fiber-to-Chip Coupler

Fig. 14. Transformation optics fiber-to-waveguide coupler design, fabrication, and characterization. (a) Grid illustrating the positioning of air holes in silicon to achieve the desired permittivity profile, which is overlaid in color. Color scale bar calibrates permittivity values. (b) Scanning-electron microscope image of transformation optics coupler. (c) Electric field (Ey) snapshot of the transformation-optical coupler with 110 nm holes demonstrating efficient in-plane mode conversion (top view). (d) Experimental transmission through the couplers: transformation optics coupler (w. holes), transformation optics coupler outline without holes (w/o holes), and butt-coupled waveguide with no coupler (butt coupling). Adapted from [28].

While optical modulators are important components in optical interconnects, efficient couplers to bring source light from a fiber-coupled laser to a bus waveguide are also required, among other essential components. We employed a transformation optics approach to design a compact fiber-to-chip coupler that can be fabricated with a single-step lithography process simultaneously with the optical modulator [28]. As shown in Fig. 14, our design minimizes coupling losses by efficiently and compactly converting the effective mode size from a larger fiber mode to the smaller waveguide mode. In the design of the coupler, a coordinate transformation is performed wherein spatial variations of the refractive index are used to compress the mode profile resulting in near perfect in-plane mode conversion; the desired permittivity profile is achieved by employing a hexagonal lattice of fixed diameter sub-wavelength air holes with varying filling fraction. Both the finite element method and finite-difference time domain simulations were performed to design and simulate the performance of the coupler. Figure 14d shows the experimentally measured transmission of the fabricated transformation optics coupler (w. holes) in comparison to butt coupling (i.e., no coupler between the fiber and the on-chip waveguide), as well as transmission using the transformation optics coupler design without holes (w/o holes). The transformation optics coupler exhibits a factor of 5 improvement in transmission efficiency over butt coupling for fiber-to-waveguide mode conversion. It is important to highlight that this result is achieved with a coupler that is only 10 microns in length, significantly more compact than traditional tapered coupler designs.

-15-

Interestingly, the coupler outline (no holes) also performs well. Given its simpler fabrication without the submicron sized holes, this coupler design is even more straightforward to integrate with on-chip silicon photonic components.

Slotted photonic crystal nanobeam

Beyond the hybrid Si-VO$_2$ ring resonators and absorption modulator designs, we also considered alternative configurations with enhanced light-matter interaction that could be used for optical switching. As shown in Fig. 15, by combining a slot waveguide and a one-dimensional photonic crystal, it is possible to produce strong localized field enhancements [29, 30]. The fundamental cavity mode supported by the slotted photonic crystal nanobeam cavity features localized field enhancements within the slot region between air holes. This "pinched" field distribution significantly reduces the cavity mode volume. The slotted photonic crystal nanobeam cavity achieved a record low mode volume V ~ 0.01$(\lambda/n)^3$ and an experimental quality factor near 10^4 [30]. The strong field confinement and low mode volumes afforded by this geometry offer the potential for developing ultracompact Si-VO2 hybrid structures with very low energy requirements.
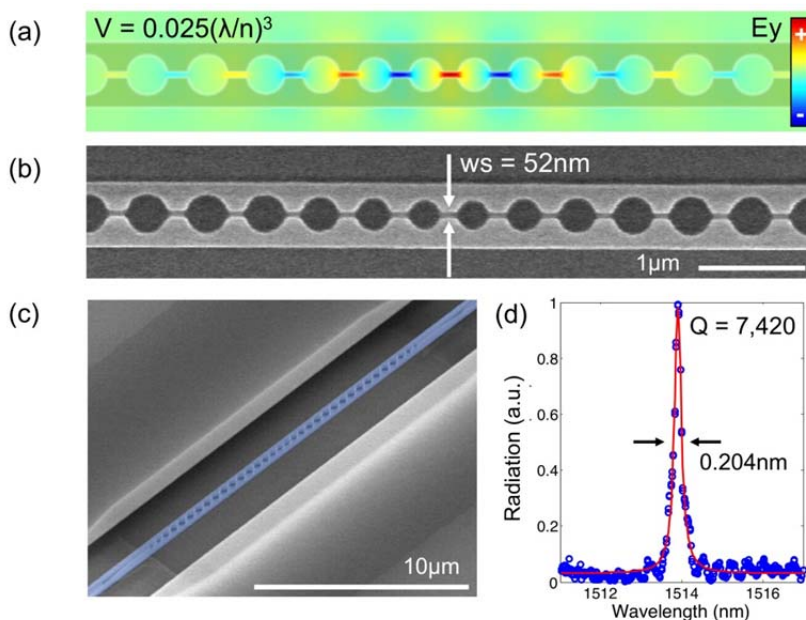

Fig. 15 (a) 3D FDTD simulated near field distribution for slotted photonic crystal nanobeam cavity mode with low V = 0.025$(\lambda/n)^3$ and high Q = 35,000. (b, c) SEM images of a fabricated device. (d) Experimentally measured cavity resonance revealing Q = 7,420.

Hybrid Si-VO$_2$-Au Plasmonic Modulator

In order to further increase modulation depth and decrease the footprint of electrically tunable Si-VO$_2$ optical modulators, we considered the incorporation of plasmonic elements and assessed the performance of the new hybrid modulator through simulation. Figure 16a shows the design of our hybrid Si-VO$_2$-Au plasmonic modulator with silicon as a bottom layer, VO$_2$ as the active layer in the middle, and gold nanodisks on top [31]. The gold nanoparticle chain is chosen to facilitate a compact footprint and regions of very high electric field confinement where the active material, VO$_2$, can be switched. Fig. 16b shows the electric field distribution of the fundamental quasi-TM plasmonic mode for this structure, confirming that most of the mode is

confined within the VO$_2$ layer to maximize the extinction ratio of the modulator and allow lower-loss propagation of the hybrid plasmonic mode in the semiconducting VO$_2$ film. When VO$_2$ is switched into a metallic state (Fig. 16c), the hybrid mode no longer propagates and the loss is significantly increased, resulting in signal modulation.
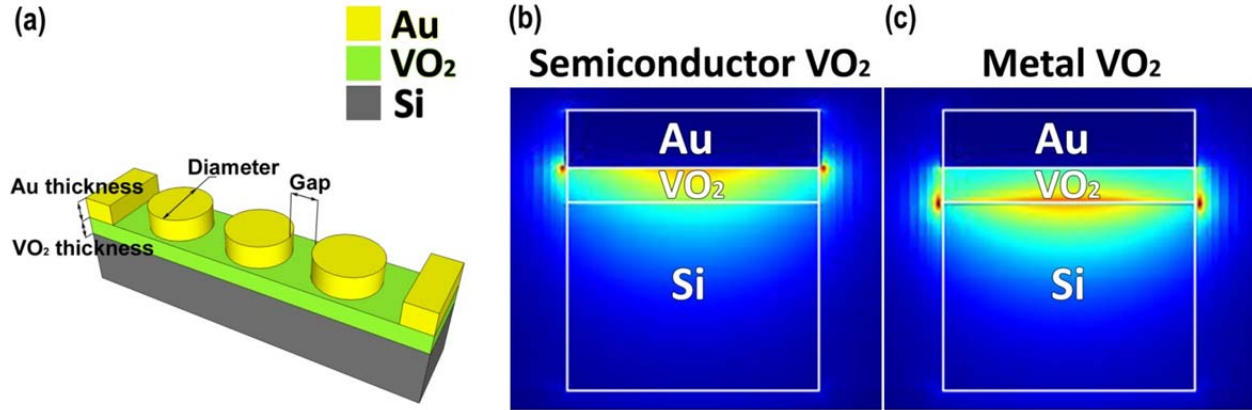

Fig. 16. (a) Schematic representation of the proposed hybrid plasmonic modulator design based on Au, VO$_2$, and Si. Electric field intensity of the hybrid mode for VO$_2$ in the (b) semiconducting state and (c) metallic state. Adapted from [31].

The hybrid Si-VO$_2$-Au plasmonic modulator exhibited excellent simulated performance in several important categories, including ultra-small footprint (560 nm × 200 nm), extinction ratio per unit length (~9 dB/μm), and operating power (4.8 mW) [31]. With the potential for direct integration into silicon waveguides, this new design is expected to dramatically improve the performance of silicon electro-optic modulators.

The research results described in this report were disseminated in the publications and at the conferences specified below.

Publications:

1) P. Markov, R. E. Marvel, H. J. Conley, K. J. Miller, K. Bolotin, R. F. Haglund, and S. M. Weiss, "Investigation of electrically induced phase transition in VO$_2$ via a hybrid Si-VO$_2$ electro-optic modulator," Manuscript in preparation.

2) P. Markov, K. Appavoo, R. F. Haglund, and S. M. Weiss, "Hybrid Si-VO$_2$-Au modulator based on near-field plasmonic coupling," Manuscript in preparation.

3) J. D. Ryckman, K. A. Hallman, R. E. Marvel, R. F. Haglund, and S. M. Weiss, "Ultra-compact silicon photonic devices reconfigured by an optically induced semiconductor-to-metal transition," Opt. Express 21, 10753-10763 (2013).

4) P. Markov, J. D. Ryckman, R. E. Marvel, K. A. Hallman, R. F. Haglund, and S. M. Weiss, "Silicon-VO$_2$ hybrid electro-optic modulator," in CLEO: Science and Innovations, OSA Technical Digest (Optical Society of America, 2013), paper CTu2F.7.

5) Judson D. Ryckman, "Porous and phase change nanomaterials for photonic applications," Ph.D. thesis, Vanderbilt University, May 2013.

6) J. D. Ryckman and S. M. Weiss, "Low mode volume slotted photonic crystal single nanobeam cavity," Appl. Phys. Lett. 101, 071104 (2012). [Cover article, selected to be highlighted in "Optics in 2013" special issue of Optics & Photonics News]

7) P. Markov, J. G. Valentine, and S. M. Weiss, "Fiber-to-chip coupler designed using an optical transformation," Opt. Express 20, 14705-14713 (2012).

8) J. D. Ryckman, V. Diez-Blanco, J. Nag, R. E. Marvel, B. K. Choi, R. F. Haglund, Jr., and S. M. Weiss, "Photothermal optical modulation of ultra-compact hybrid Si-VO2 ring resonators," Opt. Express 20, 13215-13225 (2012).

9) J. D. Ryckman and S. M. Weiss, "Localized field enhancements in guided and defect modes of a periodic slot waveguide," IEEE Photonics J. 3, 986-995 (2011).

10) P. Markov, J. G. Valentine, and S. M. Weiss, "Fiber-to-chip coupler based on transformation optics," in CLEO: QELS-Fundamental Science, OSA Technical Digest (Optical Society of America, 2012), paper QM1C.2.

Conference Presentations:
1) P. Markov, G. A. Rodriguez, J. W. Mares, R. E. Marvel, R. F. Haglund, and S. M. Weiss, "Silicon photonics for biosensing and reconfigurable photonics applications," Center for Nanophase Materials Sciences Annual Users Meeting, Oak Ridge National Laboratory, Oak Ridge, TN, Sept. 2014.

2) P. Markov, J. D. Ryckman, R. E. Marvel, K. A. Hallman, R. F. Haglund, and S. M. Weiss, "Silicon-VO_2 hybrid electro-optic modulator," Conference on Lasers and Electro-Optics (CLEO), San Jose, CA, June 2013.

3) S. M. Weiss, "Low mode volume active regions in silicon photonic cavities for low power, ultrafast switching," Materials Research Society, Boston, MA, Nov. 2012. (invited presentation)

4) S. Hu, J. D. Ryckman, Y. Jiao, J. W. Mares, V. Diez-Blanco, R. E. Marvel, R. F. Haglund and S. M. Weiss, "Nanophotonics: From novel fabrication technologies to reconfigurable photonics," Center for Nanophase Materials Sciences Annual Users Meeting, Oak Ridge National Laboratory, Oak Ridge, TN, Sept. 2012.

5) J. D. Ryckman, V. Diez-Blanco, J. Nag, R. E. Marvel, B. K. Choi, R. F. Haglund, and S. M. Weiss, "Photothermal optical switching in ultra-compact hybrid Si VO_2 ring resonators," IEEE Group IV Photonics, San Diego, CA, August 2012. [J. D. Ryckman received the top award for the student paper competition]

6) J. D. Ryckman and S. M. Weiss, "Low mode volume slotted photonic crystal single nanobeam cavity in silicon," IEEE Group IV Photonics, San Diego, CA, August 2012.

7) P. Markov, J. G. Valentine, and S. M. Weiss, "Fiber-to-chip coupler based on transformation optics," Conference on Lasers and Electro-Optics (CLEO), San Jose, CA, May 2012.

8) S. M. Weiss, "Hybrid nanoscale material systems for advanced optical performance in sensing and computing," Chemical and Biological Engineering Department Seminar Series, University of Alabama, Tuscaloosa, AL, Feb. 2012. (invited presentation)

9) J. D. Ryckman, J. Nag, C. Kang, T. E. Whittle, P. Markov, B. K. Choi, R. F. Haglund, Jr., and S. M. Weiss, "Si-VO_2 hybrid photonic structures for optical modulation and reconfigurable photonic networks," Materials Research Society Spring Meeting, San Francisco, CA, Apr. 2011.

References

[1] J. D. Ryckman, V. Diez-Blanco, J. Nag, R. E. Marvel, B. K. Choi, R. F. Haglund, S. M. Weiss, "Photothermal optical modulation of ultra-compact hybrid Si-VO$_2$ ring resonators," Optics Express **20**, 13215-13225 (2012).

[2] J. Nag, E. A. Payzant, K. L. More, R. F. Haglund, Jr., "Enhanced performance of room-temperature-grown epitaxial thin films of vanadium dioxide," Applied Physics Letters **98**, 251906 (2011).

[3] G. Cocorullo, F. G. Della Corte, I. Rendina, P. M. Sarro, "Thermo-optic effect exploitation in silicon microstructures," Sensors and Actuators A: Physical **71**, 19-26 (1998).

[4] A. Liu, R. Jones, L. Liao, D. Samara-Rubio, D. Rubin, O. Cohen, R. Nicolaescu, M. Paniccia, "A high-speed silicon optical modulator based on a metal-oxide-semiconductor capacitor," Nature **427**, 615-618 (2004).

[5] T. Ben-Messaoud, G. Landry, J. P. Gariépy, B. Ramamoorthy, P. V. Ashrit, A. Haché, "High contrast optical switching in vanadium dioxide thin films," Optics Communications **281**, 6024-6027 (2008).

[6] E. Dulkeith, F. Xia, L. Schares, W. M. J. Green, Y. A. Vlasov, "Group index and group velocity dispersion in silicon-on-insulator photonic wires," Optics Express **14**, 3853-3863 (2006).

[7] J. D. Ryckman, *Porous and phase change nanomaterials for photonic applications*, (Vanderbilt University 2013).

[8] J. D. Ryckman, K. A. Hallman, R. E. Marvel, R. F. Haglund, S. M. Weiss, "Ultra-compact silicon photonic devices reconfigured by an optically induced semiconductor-to-metal transition," Optics Express **21**, 10753-10763 (2013).

[9] M. H. D. Wegkamp, L. Xian, M. Gatti, P. Cudazzo, C. L. McGahan, R. E. Marvel, R. F. Haglund, Jr., A. Rubio, M. Wolf and J. Stähler, "Instantaneous band-gap collapse in photoexcited monoclinic VO$_2$ due to photocarrier doping," Physical Review Letters **114**, 216401 (2014).

[10] R. M. Briggs, I. M. Pryce, H. A. Atwater, "Compact silicon photonic waveguide modulator based on the vanadium dioxide metal-insulator phase transition," Optics Express **18**, 11192-11201 (2010).

[11] A. Cavalleri, T. Dekorsy, H. H. W. Chong, J. C. Kieffer, R. W. Schoenlein, "Evidence for a structurally-driven insulator-to-metal transition in VO$_2$: A view from the ultrafast timescale," Physical Review B **70**, 161102 (2004).

[12] M. Liu, X. Yin, E. Ulin-Avila, B. Geng, T. Zentgraf, L. Ju, F. Wang, X. Zhang, "A graphene-based broadband optical modulator," Nature **474**, 64-67 (2011).

[13] T. Liang, L. Nunes, T. Sakamoto, K. Sasagawa, T. Kawanishi, M. Tsuchiya, G. Priem, D. Van Thourhout, P. Dumon, R. Baets, H. Tsang, "Ultrafast all-optical switching by cross-absorption modulation in silicon wire waveguides," Optics Express **13**, 7298-7303 (2005).

[14] Q. Xu, B. Schmidt, S. Pradhan, M. Lipson, "Micrometre-scale silicon electro-optic modulator," Nature **435**, 325-327 (2005).

[15] R. Lopez, R. F. Haglund, L. C. Feldman, L. A. Boatner, T. E. Haynes, "Optical nonlinearities in VO$_2$ nanoparticles and thin films," Applied Physics Letters **85**, 5191-5193 (2004).

[16] A. Cavalleri, C. Toth, C. W. Siders, J. A. Squier, F. Raksi, P. Forget, J. C. Kieffer, "Femtosecond structural dynamics in VO$_2$ during an ultrafast solid-solid phase transition," Physical Review Letters **87**, 237401 (2001).

[17]V. R. Morrison, R. P. Chatelain, K. L. Tiwari, A. Hendaoui, A. Bruhacs, M. Chaker, B. J. Siwick, "A photoinduced metallic phase of monoclinic vanadium dioxide," arXiv1407.1304 (2014).

[18]Z. S. Tao, T. R. T. Han, S. D. Mahanti, P. M. Duxbury, F. Yuan, C. Y. Ruan, K. Wang, J. Q. Wu, "Decoupling of Structural and Electronic Phase Transitions in VO_2," Physical Review Letters **109**, 166406 (2012).

[19]G. Stefanovich, A. Pergament, D. Stefanovich, "Electrical switching and Mott transition in VO_2," Journal of Physics-Condensed Matter **12**, 8837-8845 (2000).

[20]B.-G. Chae, H.-T. Kim, D.-H. Youn, K.-Y. Kang, "Abrupt metal–insulator transition observed in VO_2 thin films induced by a switching voltage pulse," Physica B: Condensed Matter **369**, 76-80 (2005).

[21]J. S. Brockman, L. Gao, B. Hughes, C. T. Rettner, M. G. Samant, K. P. Roche, S. S. P. Parkin, "Subnanosecond incubation times for electric-field-induced metallization of a correlated electron oxide," Nature Nanotechnology **9**, 453-458 (2014).

[22]M. K. Liu, H. Y. Hwang, H. Tao, A. C. Strikwerda, K. B. Fan, G. R. Keiser, A. J. Sternbach, K. G. West, S. Kittiwatanakul, J. W. Lu, S. A. Wolf, F. G. Omenetto, X. Zhang, K. A. Nelson, R. D. Averitt, "Terahertz-field-induced insulator-to-metal transition in vanadium dioxide metamaterial," Nature **487**, 345-348 (2012).

[23]P. Markov, R. E. Marvel, H. J. Conley, K. J. Miller, K. Bolotin, R. F. Haglund, S. M. Weiss, "Investigation of electrically induced phase transition in VO_2 via a hybrid Si-VO_2 electro-optic modulator," Manuscript in preparation.

[24]M. Rini, A. Cavalleri, R. W. Schoenlein, R. López, L. C. Feldman, J. R. F. Haglund, L. A. Boatner, T. E. Haynes, "Photoinduced phase transition in VO_2 nanocrystals: ultrafast control of surface-plasmon resonance," Optics Letters **30**, 558-560 (2005).

[25]Z. You, C. Xiaonan, K. Changhyun, Y. Zheng, C. Mouli, S. Ramanathan, "Voltage-Triggered Ultrafast Phase Transition in Vanadium Dioxide Switches," Electron Device Letters, IEEE **34**, 220-222 (2013).

[26]A. Pashkin, C. Kubler, H. Ehrke, R. Lopez, A. Halabica, R. F. Haglund, R. Huber, A. Leitenstorfer, "Ultrafast insulator-metal phase transition in VO_2 studied by multiterahertz spectroscopy," Physical Review B **83**, 195120 (2011).

[27]M. Rini, Z. Hao, R. W. Schoenlein, C. Giannetti, F. Parmigiani, S. Fourmaux, J. C. Kieffer, A. Fujimori, M. Onoda, S. Wall, A. Cavalleri, "Optical switching in VO_2 films by below-gap excitation," Applied Physics Letters **92**, 181904 (2008).

[28]P. Markov, J. G. Valentine, S. M. Weiss, "Fiber-to-chip coupler designed using an optical transformation," Optics Express **20**, 14705-14713 (2012).

[29]J. D. Ryckman, S. M. Weiss, "Localized Field Enhancements in Guided and Defect Modes of a Periodic Slot Waveguide," IEEE Photonics Journal **3**, 986-995 (2011).

[30]J. D. Ryckman, S. M. Weiss, "Low mode volume slotted photonic crystal single nanobeam cavity," Applied Physics Letters **101**, 071104 (2012).

[31]P. Markov, K. Appavoo, R. F. Haglund, S. M. Weiss, "Hybrid Si-VO_2-Au modulator based on near-field plasmonic coupling," Manuscript in preparation.